



## Space charge distributions in insulating polymers: A new non-contacting way of measurement

D. Marty-Dessus, A. C. Ziani, A. Petre, and L. Berquez

Citation: *Review of Scientific Instruments* **86**, 043905 (2015); doi: 10.1063/1.4919008

View online: <http://dx.doi.org/10.1063/1.4919008>

View Table of Contents: <http://scitation.aip.org/content/aip/journal/rsi/86/4?ver=pdfcov>

Published by the [AIP Publishing](#)

---

### Articles you may be interested in

On the dynamics of the space-charge layer inside the nozzle of a cutting torch and its relation with the “non-destructive” double-arching phenomenon

*J. Appl. Phys.* **110**, 083302 (2011); 10.1063/1.3651398

Millisecond time-range analysis of space-charge distribution and electroluminescence in insulating polymers under transient electric stress

*J. Appl. Phys.* **98**, 093528 (2005); 10.1063/1.2128050

Temperature dependence of the space-charge distribution in injection limited conjugated polymer structures

*J. Appl. Phys.* **91**, 9225 (2002); 10.1063/1.1474612

Spatial distribution of space charge in conjugated polymers

*Appl. Phys. Lett.* **79**, 779 (2001); 10.1063/1.1391399

Reflection electro-optical measurements on electroluminescent polymer films: A good tool for investigating charge injection and space charge effects

*J. Appl. Phys.* **83**, 7886 (1998); 10.1063/1.367966

---



### 'On the way to a graphene spin field effect transistor'

by Prof. Barbaros and the Özyilmaz Group at National University of Singapore



\*The Business of Science

[Download a FREE application note](#)

# Space charge distributions in insulating polymers: A new non-contacting way of measurement

D. Marty-Dessus,<sup>1,2,a)</sup> A. C. Ziani,<sup>1,2</sup> A. Petre,<sup>3</sup> and L. Berquez<sup>1,2</sup>

<sup>1</sup>Université de Toulouse, UPS, LAPLACE, 118 route de Narbonne, F-31062 Toulouse, France

<sup>2</sup>CNRS, LAPLACE, F-31062 Toulouse, France

<sup>3</sup>Université de Pau et des Pays de l'Adour, SIAME, IPRA, 2 avenue du Président Pierre Angot, F-64053 Pau, France

(Received 11 February 2015; accepted 9 April 2015; published online 24 April 2015)

A new technique for the determination of space charge profiles in insulating polymers is proposed. Based on the evolution of an existing thermal wave technique called Focused Laser Intensity Modulation Method ((F)LIMM), it allows non-contact measurements on thin films exhibiting an internal charge to be studied. An electrostatic model taking into account the new sample-cell geometry proposed was first developed. It has been shown, in particular, that it was theoretically possible to calculate the internal charge from experimental measurements while allowing an evaluation of the air layer appearing between the sample and the electrode when non-contact measurements are performed. These predictions were confirmed by an experimental implementation for two thin polymer samples (25  $\mu\text{m}$ -polyvinylidenefluoride and 50  $\mu\text{m}$ -polytetrafluoroethylene (PTFE)) used as tests. In these cases, minimum air-layer thickness was determined with an accuracy of 3% and 20%, respectively, depending on the signal-to-noise ratio during the experimental procedure. In order to illustrate the reachable possibilities of this technique, 2D and 3D cartographies of a negative space charge implanted by electron beam within the PTFE test sample were depicted: like in conventional (F)LIMM, a multidimensional representation of a selectively implanted charge remains possible at a few microns depth, but using a non-contacting way of measurement. © 2015 AIP Publishing LLC. [<http://dx.doi.org/10.1063/1.4919008>]

## I. INTRODUCTION

Reliability and proper functioning of electrical devices or integrated systems heavily rely on electrical and chemical properties of materials they are made of. Thus, a widespread cause of failure of such systems is related to the dielectric breakdown of insulations. Although these materials show a natural threshold beyond which a breakdown can occur, other extrinsic sources exist and contribute to their premature ageing, leading to an abnormal acceleration of the degradation process.

These external sources can be multiple and of very different origins but their cumulative effects converge to create an unexpected internal electric field, whose local strengths can often be lower than the theoretical breakdown value of a “perfect” insulating material. This field is directly the result of charge accumulations (electrons and holes, dipoles, ions, impurities, etc.), globally known as “space charge.” The characterization of space charge distributions in terms of nature, amount, spatial, or temporal evolution is of major importance in order to predict future behaviors, in particular ageing.<sup>1,2</sup>

In the field of dielectric materials, and more especially in polymers, many studies have been conducted trying to explain the main physical phenomena likely at the basis of charge transport or accumulation,<sup>3,4</sup> including the influence

of manufacturing processes. The understanding of charge dynamics has significantly improved because of the development of several non-destructive techniques to measure the charge profile. Space charge distribution measurement methods in dielectrics are globally classified into two main categories: thermal methods (thermal pulse,<sup>5–8</sup> thermal wave,<sup>9–11</sup> and thermal step<sup>12</sup>) and acoustic methods (pressure pulse<sup>13–16</sup> and electro-acoustic<sup>17,18</sup>). General reviews of space charge profile measurement techniques have been detailed in Refs. 19 and 20, and more specific developments in thermal techniques recently published in Ref. 21.

Polymer insulations are widely used in many different engineering applications. Most of the time, at the research lab level, each side of a thin film polymer sample is coated by a metallic electrode. However, this can be a drawback in some cases, as specific parameters may have to be followed and studied. This is, for example, the case in space industry, where thin films of dielectrics constitutive of satellites and placed in orbit are exposed to radiations of all kinds, causing trapping and accumulation of electric charges and leading to surface or in-volume dielectric ruptures. For such applications, it then becomes essential not only to be able to monitor the surface potential evolutions on the polymer but also to recreate surface condition of specimen that would not be the same without a surface electrode, in particular, from an optical point of view. Moreover, measurements made through an electrical contact may be disturbing or even destructive (addition of mechanical constraints, conduction currents, injections, and relaxations at the electrodes). The benefits that can be gained from

<sup>a)</sup>Author to whom correspondence should be addressed. Electronic mail: marty@laplace.univ-tlse.fr

remote measurement are therefore obvious, as they minimize many experimental problems that cannot be avoided in more classical instrumentation setups and give potential access to new information.

The idea of measuring space charge distributions in one-side metalized thin polymer films is not new and was materialized in the late 1970s in the works of Collins<sup>5</sup> and Von Seggern<sup>22</sup> (thermal pulse), or by Sessler in 1982<sup>13</sup> (laser induced pressure pulse). In these experiments, the non-metalized side was the bottom one of the sample, and the source was exciting the top-electrode-side of the film. At that time, it was demonstrated that a signal related to the inner space charge could be recorded. In 2004, Maeno and Fukunaga<sup>23</sup> have developed for the first time an evolution of the pulsed electroacoustic (PEA) method called “Open-PEA” in which a new electrode unit was used to apply a pulsed electric field through an air-gap. But to the knowledge of the authors, no measurement on non-electroded surface sample using a thermal wave technique has been performed up to now.

In this paper, the development of a non-contacting way of space charge measurement based on an existing thermal wave technique called (F)LIMM (Focused Laser Intensity Modulation Method) is detailed. A description of basics about this thermal instrument is first given followed by theoretical developments in these new experimental conditions and related experimental results.

## II. (F)LIMM FUNDAMENTALS

### A. General principles

For the investigation of polarization or space charge distributions in polymer insulations, the LIMM technique, first described by Lang in 1981,<sup>9</sup> is widely used.<sup>24,25</sup> With this method, the sample under investigation is heated by the absorption of an intensity modulated light produced by a laser source that can be focused or not at one surface, while a pyroelectric current is measured between top and rear surfaces. The contacting sample electrode is directly heated and the heat diffuses from the respective electrode across the sample and generates the required non-affine and strongly time- and frequency-dependent temperature and thermal-expansion profile. In this approach, there is some lateral heat diffusion mostly not only in the electrode but also in the sample. The penetration depth is varied with the modulation frequency<sup>26</sup> (Figure 1).

Based on LIMM, the focused LIMM evolution, called (F)LIMM, adds another possibility of focusing the laser beam at the sample surface, and, while associated with a XY surface scanning stage, allows 2-D or 3-D representations of the information gained from the structure under study.<sup>27</sup>

Samples used are generally thin films of polymers metallized on both sides and placed in a cell for measurements and electromagnetic shielding. It is possible to add an external DC bias voltage  $V_{ht}$  (positive or negative) in order to study its influence on the behavior of the internal space charge in various configurations (applied external electric field, effect of bias polarity, charge duration, etc.), recreating conditions close to industrial use.

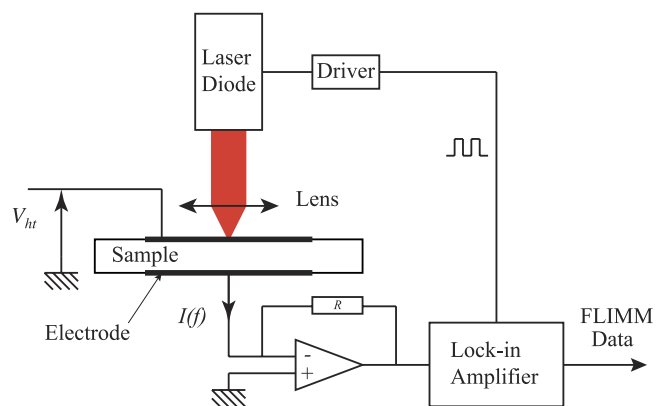


FIG. 1. (F)LIMM schematic block system.

In the presence of space charge and/or polarization in a sample, the interaction laser-material creates a pyroelectric current resulting from the rebalancing of charges on the electrodes. This current is conditioned by a transconductance amplifier, extracted from noise by a lock-in amplifier, and registered as a spectrum (real and imaginary parts) versus the modulation frequency of the beam.

The possibilities of (F)LIMM are currently a detection of space charge distribution in films of  $100 \mu\text{m}$  maximum thickness, with a lateral resolution of a few micrometers and an in-depth resolution of  $1 \mu\text{m}$  (in the direction of the sample thickness).

### B. Modeling of the electrostatic problem

To a natural or induced polarization/space charge in a sample corresponds a repartition of the pyroelectric coefficient/internal electric field.

Let us consider an internal infinitesimal planar charge  $d\sigma(\text{C m}^{-2})$  at a depth  $z$  within the sample (Figure 2). This charge influences two image charges  $\sigma_1$  and  $\sigma_2$  on both electrodes at  $z = 0$  and  $z = L$ . If the sample is submitted to an external bias  $V_{ht}$ , an additional charge  $\sigma_v$  appears, and by solving the electrostatic problem in this configuration, it is possible to establish the mathematical expression of the pyroelectric current  $I(f)$  generated by the laser-material interaction and collected between the electrodes in AC short-circuit

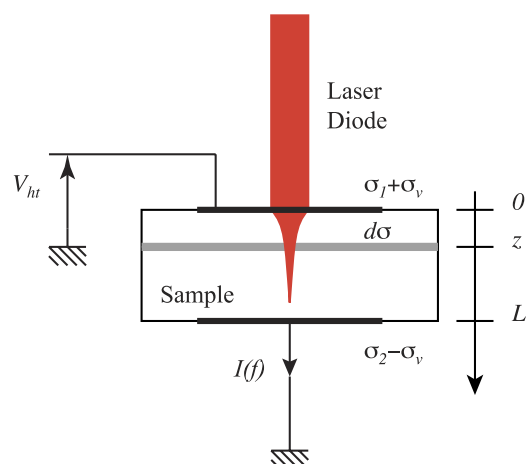


FIG. 2. (F)LIMM electrostatic problem.

conditions, such as<sup>28</sup>

$$I(f) = \int_S J(f) ds = \frac{j2\pi f}{L} \int_S \int_0^L r(z) T(z, f) dz ds, \quad (1)$$

where  $J(f)$  is the pyroelectric current density,  $S$  is the heated sample area,  $L$  its thickness,  $r(z) = p(z) - (\alpha_z - \alpha_\varepsilon) \varepsilon E(z)$ , where  $p(z)$  ( $\text{C m}^{-2} \text{K}^{-1}$ ) represents the pyroelectric coefficient for polar sample,  $\alpha_z$  and  $\alpha_\varepsilon$  ( $\text{K}^{-1}$ ) are the thermal expansion and the temperature coefficient of the permittivity, respectively.

$E(z) = E_i(z) + E_v(z)$  is the total internal electric field ( $\text{V m}^{-1}$ ),

where  $E_i(z)$  is the part of  $E(z)$  due to internal charges in the volume and  $E_v(z)$  is the part of  $E(z)$  due to  $V_{ht}$ .

For non-polar sample ( $p(z) = 0$ ), then Eq. (1) can be written as

$$\begin{aligned} I(f) &= \int_S J(f) ds \\ &= -\frac{j2\pi f}{L} \int_S \int_0^L (\alpha_z - \alpha_\varepsilon) \varepsilon E(z) T(z, f) dz ds. \end{aligned} \quad (2)$$

For polar-only samples ( $E(z) = 0$ ),

$$I(f) = \int_S J(f) ds = \frac{j2\pi f}{L} \int_S \int_0^L p(z) T(z, f) dz ds. \quad (3)$$

Starting from these expressions, it is possible to follow the evolutions of the internal field or polarization by using a suitable mathematical deconvolution. This operation is however complex: it requires not only both a full knowledge of the thermal gradient variations in the measurement cell but also an implementation of a powerful mathematical procedure, as Eq. (2) or Eq. (3) leads systematically to the solving of an ill-posed problem.<sup>29-35</sup>

### III. NON-CONTACTING MEASUREMENT: THEORY

#### A. A necessity

It was shown that it was possible to follow the repartition of the internal electric field or polarization through the knowledge of the temperature evolution in the structure under study, and different suitable models were developed to this aim. But in all cases, measurements were made with contact, as the sample was sandwiched in the measurement cell, so that no access to the variations of the surface potential was possible (this potential remaining at a given value fixed by the cell). Even if in most industrial applications needing LIMM experimentation, accessing that kind of information is not necessarily useful, it can be the case for specific studies as previously mentioned.

#### B. New developments in non-contacting (F)LIMM

In non-contacting (F)LIMM, the upper measuring electrode is deported by inserting an air-gap between the sample and it (Figure 3).

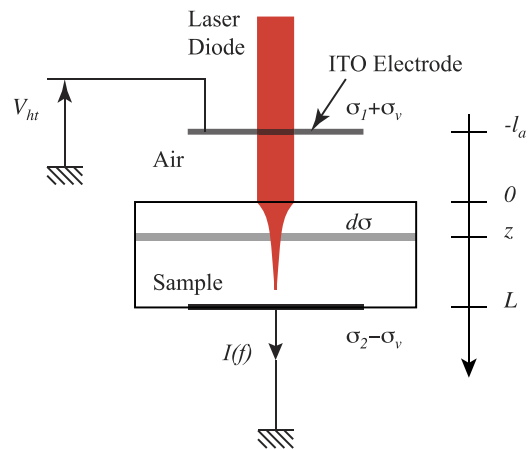


FIG. 3. Non-contacting (F)LIMM principle.

In this configuration, most of the energy of the laser is to be transmitted through a top glass slide and its transparent Indium Tin Oxide (ITO) electrode. Conversion into heat, therefore, mostly happens inside the polymer sample, and the resulting heat source is no longer a very thin layer, but its geometry is rather determined by the absorption profile of the relevant laser light. Diffusion of the heat then again leads to the required time-dependent non-affine sample deformation. In this quite different situation, both the light-absorption profile in the sample and the heat-diffusion profile are taken into account in their space and frequency dependence separately (and then combined subsequently).

To this aim, the measurement cell was considered to be composed of five different layers: top air, glass with ITO electrode, air-gap, sample (uncoated top and gold metalized rear side), and sample-holder brass back electrode. Each interface with a specific specular reflection induced a light flux with a transmitted part and a reflected one, and provided initially by the laser source. Related complex refractive indexes were determined from both experimental optical absorption measurements and the literature data. The calculation of all incident and reflected light fluxes within the five layers, including multiple reflections at interfaces, allows the determination of the heat sources from the laser in each layer and thus the corresponding evolutions of  $T_i(z, f)$  in layer  $i$ , taking into account equations of continuity between layers and boundary conditions (in our case, top layer and back electrode were both considered as semi-infinite media).

In the presence of an air layer, the global geometry to consider has also changed from an electrostatic point of view. In this new configuration, solving the problem leads to a new mathematical expression of  $I(f)$  of the form

$$\begin{aligned} I(f) &= \int_S J(f) ds \\ &= -j2\pi f \frac{\alpha}{l_a/\varepsilon_a + L/\varepsilon} \int_S \int_0^L (E_i(z) \\ &\quad + E_v(z)) T(z, f) dz ds, \end{aligned} \quad (4)$$

with  $\alpha = \alpha_z - \alpha_\varepsilon (\text{K}^{-1})$ ,  $l_a, \varepsilon_a$  is the air-layer thickness and dielectric permittivity, respectively, and  $L, \varepsilon$  is the sample thickness and dielectric permittivity, respectively.

### C. Signal evolution versus air-layer thickness

As mentioned before, the objective is to measure a pyroelectric current without direct contact between the sample and the measuring electrode. The accuracy of the internal electric field obtained after mathematical treatment depends on the proper measurement of the sample-electrode distance, and this is particularly important considering that these measurements are made on thin films ( $100 \mu\text{m}$ ).

In order to determine the thickness of the air-layer, it is important to know its relationship with the magnitude of the measured signal. If  $l_a$  is set as a parameter in Eq. (4), then

$$I(f, l_a) = -j2\pi f \frac{\alpha}{l_a/\varepsilon_a + L/\varepsilon} \int_S \int_0^L (E_i(z) + E_v(z)) T(z, f) dz ds. \quad (5)$$

For a measurement with mechanical contact, ( $l_a = 0$ ); thus,

$$I(f, 0) = -j2\pi f \frac{\alpha}{L/\varepsilon} \int_S \int_0^L (E_i(z) + E_v(z)) T(z, f) dz ds. \quad (6)$$

Assuming that the air-layer does not influence the temperature repartition in the sample, Eq. (4) becomes

$$\begin{aligned} I(f, l_a) &= \frac{L/\varepsilon}{l_a/\varepsilon_a + L/\varepsilon} I(f, 0) = \left( \frac{\varepsilon}{\varepsilon_a L} l_a + 1 \right)^{-1} I(f, 0) \\ &= \left( \frac{l_a}{L'} + 1 \right)^{-1} I(f, 0), \end{aligned}$$

where  $L' = L\varepsilon_a/\varepsilon$ .

One can deduce

$$I(f, 0) = I(f, l_a) \left( \frac{l_a}{L'} + 1 \right) \quad (7)$$

and

$$I(f, l_a)^{-1} = I(f, 0)^{-1} \left( \frac{l_a}{L'} + 1 \right). \quad (8)$$

Representative curves of  $g(l_a) = I(f, l_a)^{-1}$  are linear functions shown in Figure 4 for two given frequencies  $f_1$  and  $f_2$ .

In practice, a micrometric screw system is used to lift the cover of the cell and control the thickness of air between

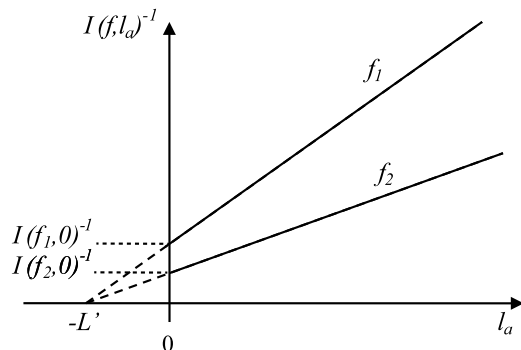


FIG. 4.  $g(l_a) = I(f, l_a)^{-1}$  theoretical curves for 2 given frequencies  $f_1$  and  $f_2$ .

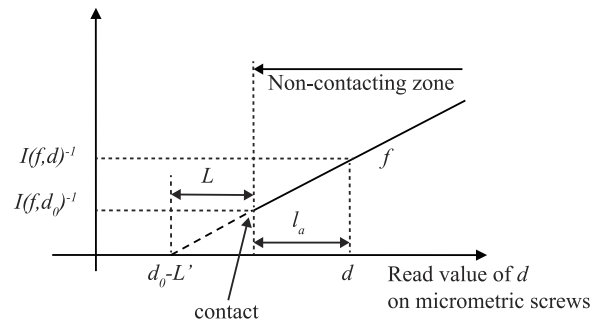


FIG. 5.  $g(d) = I(f, d)^{-1}$  theoretical curves. Introduction of  $d$  as a new variable.

the upper and the lower electrodes (Figure 6). But if a direct reading on the screws can be accurate, it does not directly correspond to the value of the thickness of the air-layer because of the existing mechanical constraints, ripples on the sample surface, or mechanical clearance.

To overcome this problem, let us consider Figure 5, where  $l_a$  is replaced by  $d$ , a new parameter representing the read values on micrometric screws.

In the non-contacting zone  $d > d_0$  and for a given frequency  $f$ , a linear variation of  $I(f, d)^{-1}$  is obtained. The

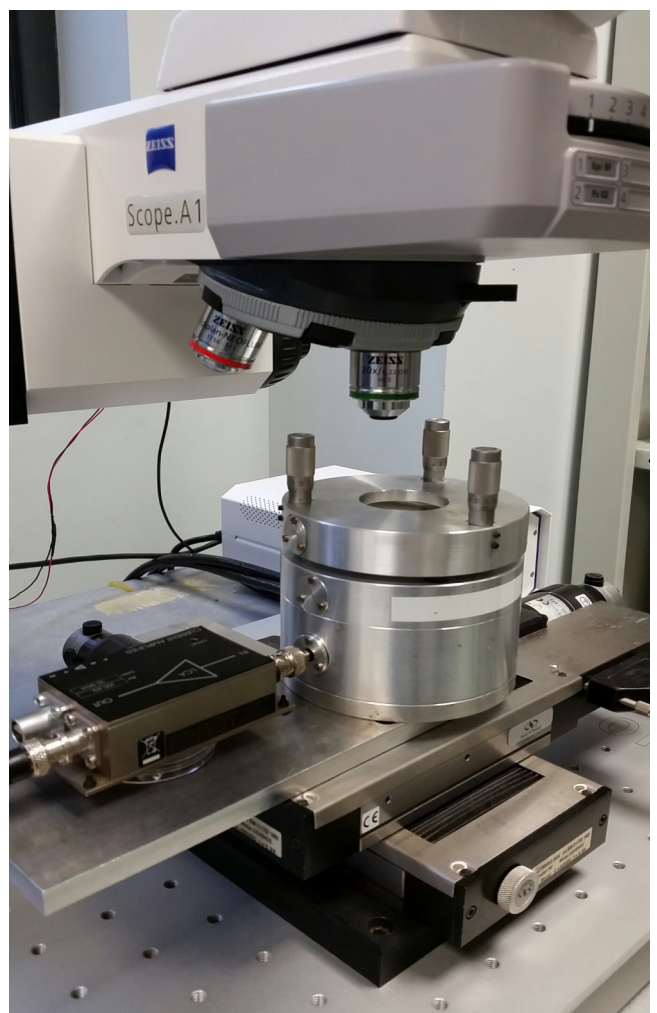


FIG. 6. Non-contacting (F)LIMM experimental setup.

air-layer thickness is given by  $l_a = d - d_0$ , if  $d_0$  is the numerical value read on the micrometric screws as the upper electrode comes to contact the sample.

Then, for  $d < d_0$ , the upper electrode is in contact with the sample, and a mechanical clearance appears between the micrometric screw extremity and the cell.  $I(f, d_0)^{-1}$  is in this case the same as in classical (F)LIMM with contact, that is, to say  $I(f, d_0)^{-1} = I(f, 0)^{-1}$ . But, in practice, it is not possible to directly figure out  $d_0$  because a measurement with contact is not wished.

Let us consider Eq. (8). Within the non-contacting zone, it can be rewritten as

$$g(d) = I(f, d)^{-1} = I(f, d_0)^{-1} \left( \frac{d - d_0}{L'} + 1 \right). \quad (9)$$

$g(d)$  can be plotted by a linear section that crosses the x-axis at  $d = d_0 - L'$ . For a given frequency, this value of  $d = d_0 - L'$  can be determined. Knowing the value of  $L'$  directly linked to the sample thickness  $L$  by  $L' = L\epsilon_a/\epsilon$ , it is then possible to calculate the value of  $d_0$ , and then of  $l_a$ .

In practice, this measurement will have to be repeated using different frequencies in order to increase the precision in the evaluation of  $d_0 - L'$ .

#### IV. EXPERIMENT

In the classic experimental (F)LIMM, the measuring cell consists of two covers: the first one used as a sample holder and directly connected to the current amplifier and the second one placed on the top of the sample and physically connected to  $V_{ht}$ , allowing to flatten the sample between two metal electrodes, with a centered hole for heat deposition by the laser source.

The main evolution in non-contacting (F)LIMM is related to the top cover: three micrometric screws were added and have the main function of lifting vertically the top electrode of glass coated by a layer of ITO (Figure 6). In these experimental conditions, a layer of air is created above the sample not flattened anymore by the top cover, while keeping valid the AC short-circuit condition and thus the extended electrostatic model.

In this configuration, we developed a new mathematical model for temperature gradient calculations in order to take into account the new geometry of the cell. These advanced models lead to choices in terms of optimal thickness of the different layers in the cell and also for sample's nature of metallization and geometry.

Test samples used were  $30 \times 20$  mm films of polar PVDF (Polyvinylidenefluoride) and electron irradiated PTFE (Polytetrafluoroethylene).

A first sample was a bi-oriented commercial PVDF film of  $25 \mu\text{m}$  ( $\epsilon_r = 9$ ). One side was coated by a thin gold layer of  $20 \text{ nm}$  and  $16 \text{ mm}$  in diameter, then placed and glued onto the rear electrode of the measurement cell using an epoxide resin. The sample was maintained blocked in the cell for a few hours in order to ensure an intimate contact with the electrode and minimize non-planarity.

A second sample of PTFE ( $\epsilon_r = 2$ ) was prepared from a TEFLO<sup>®</sup> sheet of  $50 \mu\text{m}$  thickness. Both sides were coated with a  $20 \text{ nm}$  gold layer and  $16 \text{ mm}$  in diameter. Negative charges were then implanted in the sample by the mean of a  $30 \text{ keV}$  electron-beam during  $20 \text{ min}$  (spot size:  $75 \text{ nm}$ ). After irradiation, the sample is glued onto the rear electrode of the measurement cell using a silver paint.

Experimental data were collected with a (F)LIMM setup based on an electronically modulated laser diode (PMT45/6332,  $45 \text{ mW}$ ,  $658 \text{ nm}$ , Laser Component) avoiding any ablation damage at the top of the sample.

Samples were placed in a shielded measurement cell and positioned when needed for 2D/3D-cartographies with a motorized XY translation stage (NEWPORT MM4005). A CCD camera managed the beam positioning, and a spot size of about  $5 \mu\text{m}$  in diameter can be obtained using an adapted lens (ZEISS).

The (F)LIMM current was collected between the electrodes and pre-amplified by an ultra-low-noise current amplifier (FEMTO LCA-200k), then extracted from noise by a lock-in amplifier (EG&G Stanford Research—5302), controlling at the same time the laser modulation frequency. Typical current was ranging from  $1\text{nA}_{\text{rms}}$  to  $1\text{pA}_{\text{rms}}$ , depending on the used material. The air-layer height between the top of the sample and the measuring cell electrode was controlled by a set of 3 micrometric screws fixed on the top cover of the cell.

In this study, all measurements were made with no external potential applied ( $V_{ht} = 0$ ) in order to simplify

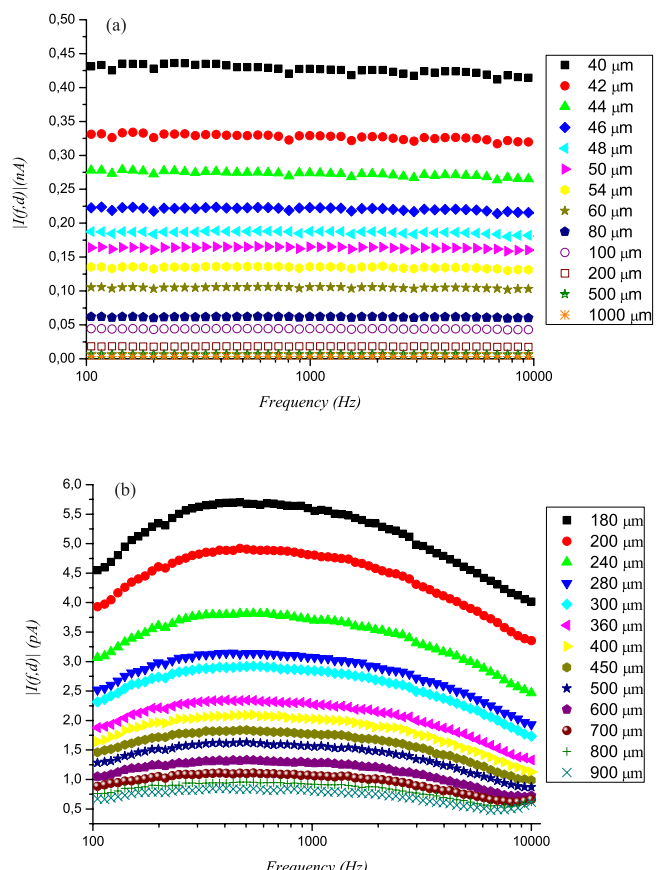


FIG. 7. Experimental current modulus vs. modulation frequency for (a) PVDF and (b) PTFE sample.

the experimental procedure, but with no influence on the global demonstration. Data acquisition was controlled by homemade software under MATLAB™ environment allowing simultaneous mathematical treatments.

Evolutions of (F)LIMM current modulus versus frequency of modulation were plotted in Figure 7 for different values of  $d$  directly read on micrometric screws.

Figures 7(a) and 7(b) correspond to results got on the PVDF and PTFE samples, respectively. Signals were recorded at 65 frequencies from 100 Hz to 10 kHz,  $d$  ranging from 40  $\mu\text{m}$  to 100  $\mu\text{m}$  for case (a), and 180 to 900  $\mu\text{m}$  for (b).

## V. DISCUSSION

### A. Air-layer thickness evaluation in non-contacting measurements

From results depicted in Figure 7, one can draw  $|I(f, d)|^{-1}$  versus  $d$  for frequencies  $f$  ranging from 105 Hz to 10 534 Hz (Figure 8(a)). The corresponding curves are linear functions, as it is the case in Eq. (9). In order to get a numerical evaluation

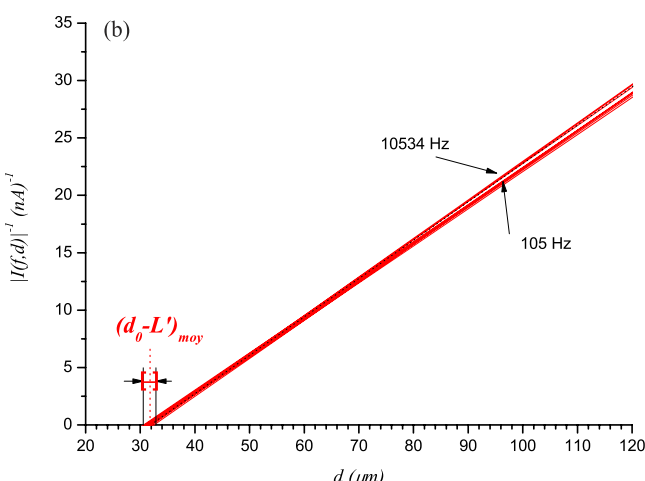
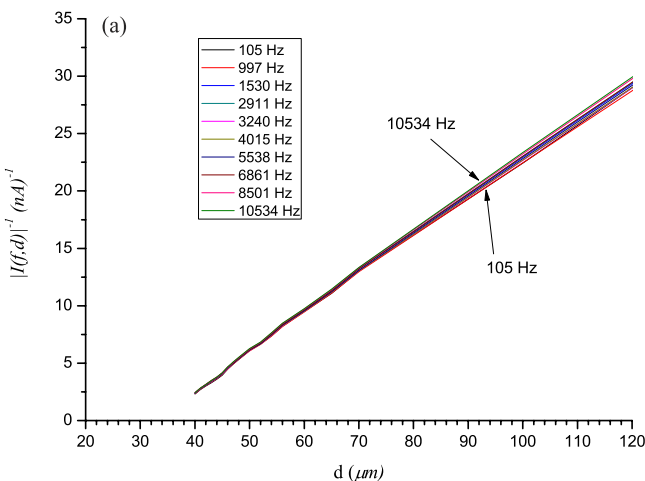


FIG. 8.  $|I(f, d)|^{-1} = g(d)$  for (a) experimental data on PVDF and (b) corresponding linear fitted curves.

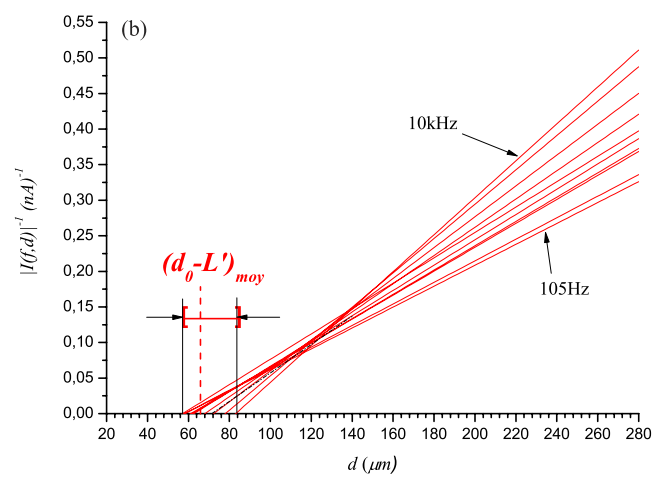
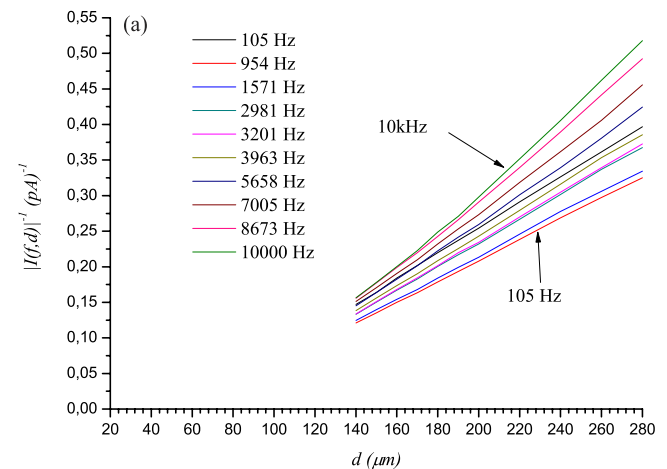


FIG. 9.  $|I(f, d)|^{-1} = g(d)$  for (a) experimental data on PTFE and (b) corresponding linear fitted curves.

of  $d_0 - L'$ , linear interpolations were needed and lead to results plotted in Figure 8(b).

Values of  $d_0 - L'$  obtained from interpolation vary between 31.5 and 32.5  $\mu\text{m}$ , for a mean value  $(d_0 - L')_{moy} = 31.6 \mu\text{m}$ . If  $L' = L/\varepsilon_r = 25/9 = 2.77 \mu\text{m}$ , then  $d_{0moy}$  can be calculated as  $d_{0moy} = L' + 31.6 \mu\text{m} \cong 34 \mu\text{m} \pm 1 \mu\text{m}$ . Thus,  $l_a$ , air layer thickness at a given measure of  $d$  read on micrometric screws is such as  $l_a = d - d_{0moy} = d - 34 \mu\text{m}$ . In this case, the low dispersion of the curves in Figure 8(a) gives

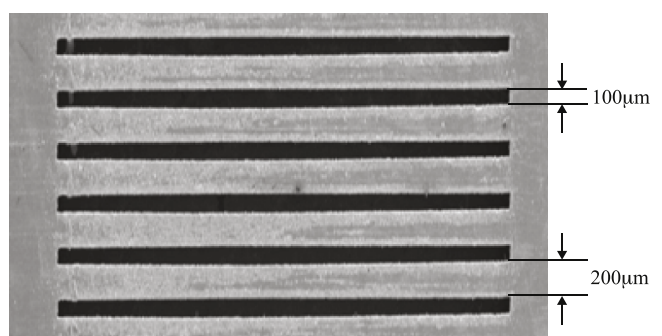


FIG. 10. Metallic grid for selective irradiation on the PTFE sample.

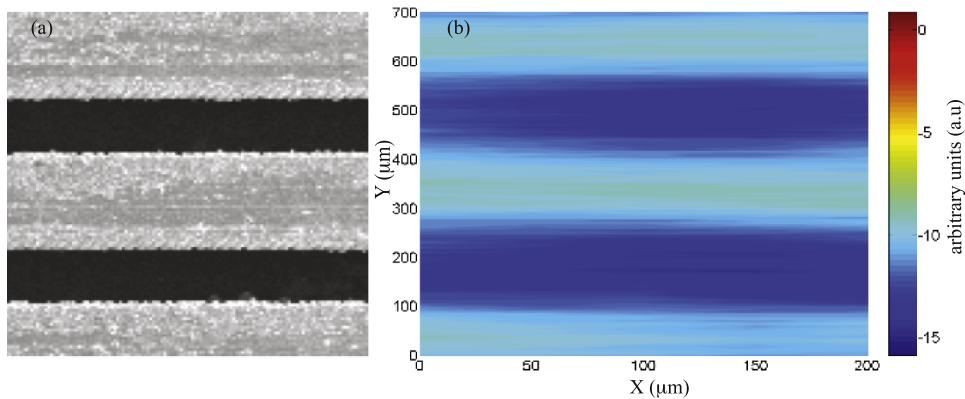


FIG. 11. 2-D cartography on the PTFE sample,  $f = 10$  kHz,  $z = 1.9 \mu\text{m}$ —(a) scanning zone (mask) and (b) image of corresponding space charge (a.u.).

a good precision of approximately 3% on the determination of the air-layer thickness.

The same procedure was repeated in the case of PTFE sample (Figure 9).

Here,  $d_0 - L'$  varies between 57.2 and 83.1  $\mu\text{m}$ , and  $(d_0 - L')_{moy} = 66.1 \mu\text{m}$ . If  $L' = L/\varepsilon_r = 50/2 = 25 \mu\text{m}$ , then  $d_0 = L' + 66.1 \mu\text{m} \approx 91 \mu\text{m} \pm 17 \mu\text{m}$  and  $l_a = d - d_{0moy} = d - 91 \mu\text{m}$ , with a precision of about 20%.

In this case, there is more dispersion on curves than in the previous example, and the precision on the determination of  $l_a$  is much lower. This is mainly due to the fact that the limit of detection is reached in our experimental chain (values of AC current below 1 pA<sub>rms</sub>) with maximal noise. Thus, the precision on air layer thickness evaluation is directly linked not only to the signal-to-noise ratio reachable by the setup but also to the intrinsic nature of the material under study, its dielectric properties (polar or not, value of  $\varepsilon_r$ ), and to the way it has been charged (irradiation conditions in particular).

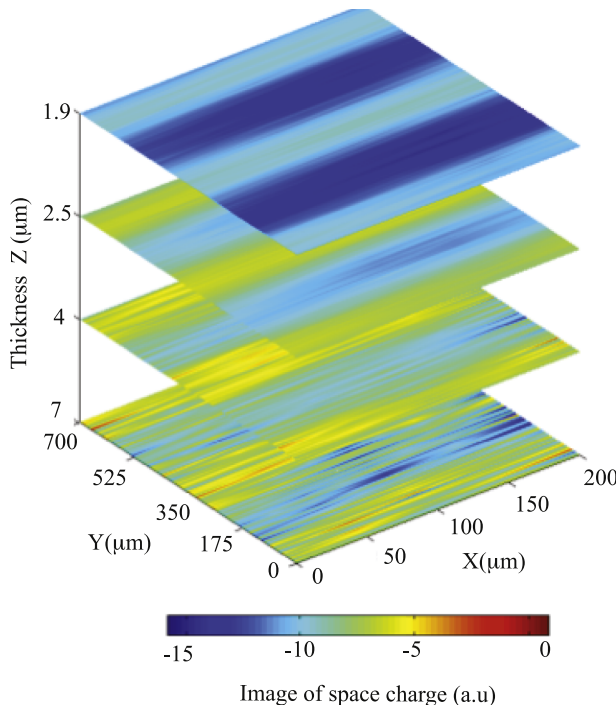


FIG. 12. 3-D cartography of space charge— $f_{max} = 10$  kHz,  $1.9 \mu\text{m} < z < 7 \mu\text{m}$ .

## B. Application: 2-D and 3-D cartographies

Recent improvements in thermal techniques made it possible to scan a sample surface, and, in association with both advanced thermal modeling and deconvolution procedures, to get multidimensional representations of space charge or polarization profiles with in-depth and lateral resolutions depending mainly on the technique considered.<sup>36–42</sup>

The first results showed that non-contacting measurements were possible, provided that significant currents can be extracted from noise. In this case, they are representative of an internal space charge (or polarization) in the sample that can be calculated by mathematical inversion of the electrostatic problem.

To illustrate the new enhanced possibilities of non-contacting (F)LIMM, it was applied to multi-dimensional cartographies of space charge and polarization.

A PTFE sample (same characteristics as in Sec. IV) was prepared for selective irradiation through a metallic mask. This metallic grid was first glued onto the sample then placed in a chamber for electron irradiation (30 keV, 20 min). Openings on the mask allow selective electron implantation with a geometry represented in Figure 10. After irradiation, the grid was removed from the sample and this one was placed in the measurement cell.

A surface scanning (rectangle of  $200 \mu\text{m} \times 700 \mu\text{m}$ ) was carried out in order to get a 2-D representation of space charge built by electronic injection. The modulation frequency was fixed at 10 kHz, corresponding to an in-depth cut at  $z = 1.9 \mu\text{m}$  (Figure 11).

Each modulation frequency of the laser fixes the size of the thermal diffusion zone and thus corresponds to a given depth within the sample. Varying this frequency leads to a possible extension to a 3-D representation<sup>19</sup> (Figure 12).

## VI. CONCLUSION

In this work, a new possibility for the study of space charge distributions in insulating polymers was proposed. Based on a technique using thermal waves as sources, the new setup allows non-destructive and contactless measurements on thin films broadly used in electrical engineering or space industry. Mathematical developments were associated with a way of theoretical evaluation of the air-layer thickness

while non-contacting measurements were first discussed. Experimental results were then indicating that it was possible to obtain a significant signal without a physical contact between the measuring electrode and the sample surface. In addition, it was shown that an estimation of the air gap appearing between the measuring cell and sample could be calculated through an original approach, and with a precision that essentially depends on the nature of the sample. This is of primary importance for the mathematical déconvolution process leading to space charge calculations.

Furthermore, multi-dimensional representations of charge evolutions in thin polymer insulations remain possible in non-contacting (F)LIMM, as it was shown on an irradiated PTFE sample. Nevertheless, complementary studies have to be conducted in order to find out what are the limitations of the technique, in particular, in terms of correlation between level of signal and maximal air thickness usable.

## ACKNOWLEDGMENTS

The authors wish to thank the anonymous reviewer for her or his suggestions and precise that they have cited the review verbatim in the second paragraph of Sec. III B.

- <sup>1</sup>L. A. Dissado, G. Mazzanti, and G. C. Montanari, *IEEE Trans. Dielectr. Electr. Insul.* **4**, 496 (1997).
- <sup>2</sup>G. Mazzanti, G. C. Montanari, and L. A. Dissado, *IEEE Trans. Dielectr. Electr. Insul.* **12**, 876 (2005).
- <sup>3</sup>L. A. Dissado, *Electrical Degradation and Breakdown in Polymers* (P. Peregrinus, London, 1992).
- <sup>4</sup>*Dielectric Materials for Electrical Engineering*, edited by J. Martínez-Vega (ISTE, Wiley, London, Hoboken, NJ, 2010).
- <sup>5</sup>R. E. Collins, *Appl. Phys. Lett.* **26**, 675 (1975).
- <sup>6</sup>R. E. Collins, *J. Appl. Phys.* **47**, 4804 (1976).
- <sup>7</sup>R. E. Collins, *Rev. Sci. Instrum.* **48**, 83 (1977).
- <sup>8</sup>R. E. Collins, *J. Appl. Phys.* **51**, 2973 (1980).
- <sup>9</sup>S. B. Lang and D. K. Das-Gupta, *Ferroelectrics* **39**, 1249 (1981).
- <sup>10</sup>S. B. Lang and D. K. Das-Gupta, *Ferroelectrics* **60**, 23 (1984).
- <sup>11</sup>S. B. Lang and D. K. Das-Gupta, *J. Appl. Phys.* **59**, 2151 (1986).

- <sup>12</sup>A. Toureille and J. P. Reboul, in *ISE6: Proceedings of the 6th International Conference on Electrets* (Oxford, England, 1988), pp. 23–27.
- <sup>13</sup>G. M. Sessler, J. E. West, and G. Gerhard, *Phys. Rev. Lett.* **48**, 563 (1982).
- <sup>14</sup>G. M. Sessler, J. E. West, R. Gerhard-Multhaup, and H. von Seggern, *IEEE Trans. Nucl. Sci.* **29**, 1644 (1982).
- <sup>15</sup>P. Laurenceau, G. Dreyfus, and J. Lewiner, *Phys. Rev. Lett.* **38**, 46 (1977).
- <sup>16</sup>C. Alquie, G. Dreyfus, and J. Lewiner, *Phys. Rev. Lett.* **47**, 1483 (1981).
- <sup>17</sup>T. Takada, T. Maeno, and H. Kushibe, *IEEE Trans. Electr. Insul.* **EI-22**, 497 (1987).
- <sup>18</sup>R. Gerhard-Multhaup, *Ferroelectrics* **75**, 385 (1987).
- <sup>19</sup>G. Sessler and R. Gerhard-Multhaup, *Radiat. Phys. Chem.* **23**, 363 (1984).
- <sup>20</sup>R. J. Fleming, *IEEE Trans. Dielectr. Electr. Insul.* **12**, 967 (2005).
- <sup>21</sup>R. Singh, *J. Electrost.* **72**, 322 (2014).
- <sup>22</sup>H. von Seggern, *Appl. Phys. Lett.* **33**, 134 (1978).
- <sup>23</sup>T. Maeno and K. Fukunaga, in *ICSD2004: Proceedings of 2004 IEEE International Conference on Solid Dielectrics*, Toulouse, France, 5–9 July 2004 (IEEE, Piscataway, NJ, USA, 2004), pp. 944–946.
- <sup>24</sup>D. K. Das-Gupta and J. S. Hornsby, *J. Phys. D: Appl. Phys.* **23**, 1485 (1990).
- <sup>25</sup>S. B. Lang, *IEEE. Trans. Dielectr. Electr. Insul.* **5**, 70 (1998).
- <sup>26</sup>S. B. Lang, *IEEE Trans. Dielectr. Electr. Insul.* **11**, 3 (2004).
- <sup>27</sup>D. Marty-Dessus, L. Berquez, A. Petre, and J. L. Franceschi, *J. Phys. D: Appl. Phys.* **35**, 3249 (2002).
- <sup>28</sup>P. Bloß and H. Schäfer, *Rev. Sci. Instrum.* **65**, 1541 (1994).
- <sup>29</sup>B. Ploss, R. Emmerich, and S. Bauer, *J. Appl. Phys.* **72**, 5363 (1992).
- <sup>30</sup>P. C. Hansen and D. P. O'Leary, *SIAM J. Sci. Comput.* **14**, 1487 (1993).
- <sup>31</sup>J. Honerkamp and J. Weese, *Continuum Mech. Thermodyn.* **2**, 17 (1990).
- <sup>32</sup>S. B. Lang, *J. Mater. Sci.* **41**, 147 (2006).
- <sup>33</sup>A. Mellinger, *Meas. Sci. Technol.* **15**, 1347 (2004).
- <sup>34</sup>A. Petre, D. Marty-Dessus, L. Berquez, and J.-L. Franceschi, *Jpn. J. Appl. Phys., Part 1* **43**, 2572 (2004).
- <sup>35</sup>S. Lang and R. Fleming, *IEEE Trans. Dielectr. Electr. Insul.* **16**, 809 (2009).
- <sup>36</sup>A. Mellinger, R. Singh, M. Wegener, W. Wirges, R. Gerhard-Multhaup, and S. B. Lang, *Appl. Phys. Lett.* **86**, 082903 (2005).
- <sup>37</sup>A. Mellinger, R. Flores-Suárez, R. Singh, M. Wegener, W. Wirges, R. Gerhard, and S. B. Lang, *Int. J. Thermophys.* **29**, 2046 (2008).
- <sup>38</sup>D. Marty-Dessus, L. Berquez, A. Petre, M. Mousseigne, and J. L. Franceschi, in *CEIDP2002: Annual Report Conference on Electrical Insulation and Dielectric Phenomena*, Cancún, Mexico, 20–24 October 2002 (IEEE, Piscataway, NJ, USA, 2002), pp. 602–605.
- <sup>39</sup>M. Stewart and M. Cain, *J. Phys.: Conf. Ser.* **183**, 012001 (2009).
- <sup>40</sup>A. Petre, C.-D. Pham, D. Marty-Dessus, and L. Berquez, *J. Electrost.* **67**, 430 (2009).
- <sup>41</sup>C.-D. Pham, A. Petre, L. Berquez, R. Flores-Suarez, A. Mellinger, W. Wirges, and R. Gerhard, *IEEE Trans. Dielectr. Electr. Insul.* **16**, 676 (2009).
- <sup>42</sup>S. Aryal and A. Mellinger, *J. Appl. Phys.* **114**, 154109 (2013).